Contents lists available at ScienceDirect

Transactions of Nonferrous Metals Society of China

36(2026) 1015−1025

www.tnmsc.cn

Mathematical modeling of grain fragmentation induced by flow shearing in high-pressure die casting of light alloys

Jing-zhou LU [a,b], Kun DOU [a,b,*], Yi-jie ZHANG [c], Ewan LORDAN [d], Alain JACOT [d], Zhongyun FAN [d], Wan-lin WANG [a]

[a] School of Metallurgy and Environment, Central South University, Changsha 410083, China;

[b] Xiangjiang Laboratory, Hunan University of Technology and Business, Changsha 410205, China;

[c] Institute for New Materials, Dongliang Aluminium Co., Ltd., Huzhou 313008, China;

[d] Brunel Centre for Advanced Solidification Technology (BCAST), Brunel University London, Kingston Lane, Uxbridge, UB8 3PH, United Kingdom

Abstract: In the cold-chamber high-pressure die casting (CC-HPDC) process for light alloys, strong shear stress generated by the fast-flowing melt through narrow runners breaks externally solidified crystals (ESCs). Two runner configurations were applied in the CC-HPDC process of aluminum alloy to address this problem. A comprehensive finite element model was established to calculate shear stress in the runner regions during die filling, and a novel mathematical model of grain breakup was proposed to quantitatively analyze ESCs fragmentation through different runners. Particles ranging in size from 12.2 to 16.1 μm constitute a significant proportion of the ESCs and serve as the primary focus of subsequent shear fragmentation. Finally, HPDC test trials validate the mathematical model by characterizing grain morphology and size distribution in as-cast samples and the error of the model is less than 20%. The results demonstrate that the novel model is highly effective for the design of runner systems and the optimization of process parameters in the CC-HPDC process for light alloys.

Keywords: externally solidified crystal (ESC); flow shearing; mathematical model; microstructure; high-pressure die casting (HPDC)

1 Introduction

The high-pressure die casting (HPDC) for light metals is a near-net-shape manufacturing approach that allows massive production and high dimension accuracy. Especially for aluminum and magnesium alloys, the cold-chamber HPDC (CC-HPDC) is widely used [1−3]. In this process, the melt is first poured into a relatively cold shot sleeve before being pushed into the die cavity with a fast-moving piston, and the mixture of melt and the partially solidified products formed in shot sleeve would flow through the relatively narrow runner and the gating system into the die cavity. And the fierce turbulence and even melt atomization would occur with the strong shear stress induced between the runner wall and the rapid-flowing melt [4]. As a result of the unsteady flow in the HPDC process, the as-cast microstructures tend to be non-uniform, and the mechanical properties of the as-cast products bear a bad reputation for poor repeatability [5].

As is studied by many researchers, the typical microstructures of HPDC components consist of a fine-grain skin region, a coarse grain central region and a porosity-containing defect band between them [6−9]. The fine grains nucleate and form in the die cavity due to high cooling rate and the coarse grains,

Corresponding author: *Kun DOU, Tel: +86-17600802394, E-mail: Kun.Dou@csu.edu.cn

https://doi.org/10.1016/S1003-6326(25)67013-0

Received 24 July 2024; accepted 27 March 2025

which are usually termed as externally solidified crystals (ESCs), primarily nucleate and grow in the shot sleeve and continue their growth into the die after being sheared and injected with melt flow. According to the Hall−Petch relationship [10], the strength of the materials would increase with decreasing grain size, so it is beneficial to refining the grains in HPDC process for better repeatability and improved mechanical properties [11,12]. So far, grain refinement in casting of light alloys has been achieved through multiple methods such as addition of grain refiners [13,14], melt quenching [15], and cavitation processing [16]. Specially, utilizing the powerful effect of flow shearing force during mechanical stirring, the intensive melt shearing technology has been developed in BCAST, Brunel [17,18] to break and disperse the formed oxides during casting process, thus promoting the heterogeneous nucleation in the solidification stage. This technology gives us a hint that if the shearing effect in the runner and gating system could be properly used, the shearing technology could be further extended and well compensated for industrial applications [19,20].

Research on flow shearing behavior in the die filling stage of the HPDC process is not rare [21]. GUNASEGARAM et al [22,23] studied the HPDC process of CA313 alloy using a prolonged runner and gating system and found that it encouraged the shearing of the melt during the die filling stage and led to more refined microstructure, less ESCs and reduced porosities. WANG and XIONG [24] studied the influence of piston shot speed on the evolution of ESCs in HPDC of AM60B magnesium alloy and found that under a low slow shot speed, large ESCs are found in the cast structure while a high fast shot speed resulted in more spherical ESCs.

LI et al [25] studied the effect of runner and gating system on the mechanical properties of HPDC AZ91D magnesium alloy and found that the ESCs were broken and eliminated by the shear stress caused by the turbulent melt with the modified gating system. Meanwhile, they proposed the addition of ESC collector in the runner region during the vacuum HPDC process of Mg−3.0Nd−0.3Zn−0.6Zr alloy and improved the casting quality by eliminating the size distribution of large ESCs in the casting part [26]. In another research work from JIAO et al [27], a new ceramic type shot sleeve was used to eliminate large-size ESCs and the mechanical properties of the AlMg6Si2MnZr alloy fabricated by CC-HPDC are improved obviously. From the above references, it could be concluded that reducing the ESCs size is proven to be beneficial to the improvement of the microstructure and the mechanical properties of the CC-HPDC products.

In the CC-HPDC process, the mechanism of ESC fragmentation induced by strong shear stress from fast-flowing melt through narrow runners has not been systematically quantified or modeled. For the first time, this study develops a novel mathematical model to quantitatively analyze the shear-induced fragmentation of ESCs with different runner designs. Compared to existing research, the model integrates a multiphysics coupling of flow field characteristics and grain dynamics, enabling more accurate predictions of grain morphology and size distribution.

The results validate the model's accuracy in practical die-casting processes and offer significant theoretical guidance for runner system design and process parameter optimization. This research addresses a critical gap in the quantitative analysis of ESC fragmentation in CC-HPDC processes, contributing to the advancement and optimization of high-performance light alloy casting technologies.

2 Experimental

2.1 Shot sleeve pre-filling experiments

To study the initial solidification of the melt in the shot sleeve, a pouring test using Al−Si alloy was conducted in the shot sleeve of a 4500 kN cold chamber HPDC machine, as shown in Fig. 1. LM24 alloy (8.09 wt.% Si, 3.11 wt.% Cu, 1.78 wt.% Zn, 0.86 wt.% Fe, 0.22 wt.% Mn, 0.16 wt.% Mg and 0.04 wt.% Ti) was used as a base material. A dose of 750 g melt was poured with an initial temperature of 680 ℃ and the time duration of 3 s. In the meantime, 8 K-type thermocouples were placed in various locations of the shot sleeve, as indicated in Fig. 1.

After the casting trials, the fully solidified products in the shot sleeve were cut, polished and etched using standard sample preparation techniques and the solidification structure was observed using scanning electron microscope (SEM). Grain size distribution was analyzed using image software. The thermal profile combined with grain size distribution were used for microstructure simulation calibrations. The grain size for ESC prior to injection was

estimated based on a fitting curve between grain size and cooling rate. The cooling rate at the time before injection was extracted based on FEM simulation for shot sleeve.

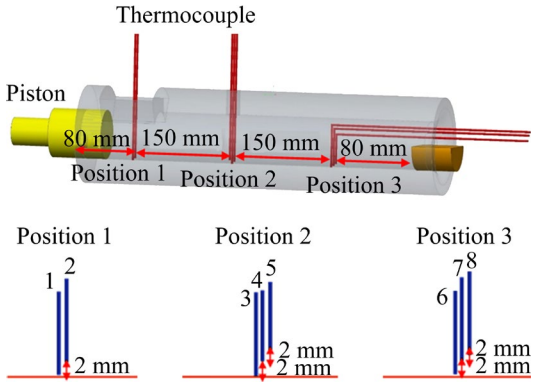

Fig. 1 Shot sleeve configuration and locations for 8 K-type thermocouples

2.2 High-pressure die casting experiments with two sets of runners

Two sets of runner and gating system were designed for the CC-HPDC process of LM24 alloy. Standard tensile samples were cast, and two groups of HPDC experiments were conducted based on the same set of process parameters, as indicated in Table 1.

Specifically, the melt was degassed using a commercial rotary degassing unit and then manually poured into the shot chamber of a Frech 4500 kN locking force CC-HPDC machine. The pouring temperature, die temperature and shot chamber temperature were maintained at 680, 200 and 180 °C, respectively. Figure 2 presents the two dies used to produce ASTM standard E8/E8M tensile specimens.

Table 1 Thermal die cycling sequence and duration used in modelling

Process	Time node/s
Sleeve pre-filling duration	3
Piston starting to move	3.01
Die opening	10
Part ejection time	20
Die spraying start time	30
Die spraying end time	48
Die blowing start time	49
Die blowing end time	55

The two dies differ in their choice of runner system: one adopts a traditional runner system (TRS), and the other employs a lean runner system (LRS) that accelerates the liquid through a contractile flow. The plunger kinematics was fixed in the experiments, with significant speeds of 0.3 and 3.6 m/s at the slow-shot and die-filling stages, respectively.

3 Modelling

3.1 Finite element modelling of CC-HPDC process

Using the finite element method, the filling and solidification processes in a CC-HPDC machine are modeled. The 1/2 computational domain for the entire HPDC machine and a detailed view of the shot sleeve region are shown in Fig. 3. The meshes are generated with Visual Mesh module in ProCAST, with a global mesh size of 2 mm and a refined mesh size of 0.2 mm at the thin ingate section. The overall mesh number is 1×10^6.

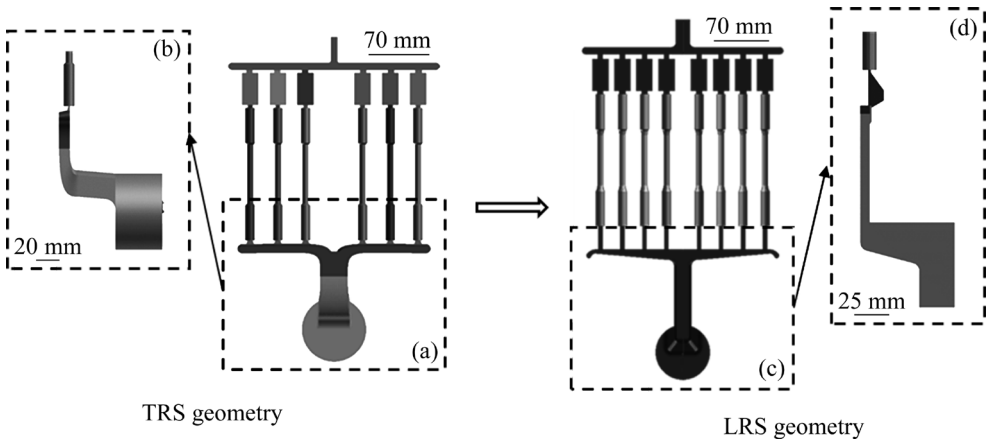

Fig. 2 Die geometries used to produce ASTM standard tensile specimens: (a, b) TRS geometry employing conventional runner; (c, d) LRS geometry with aim to accelerate liquid through flow constriction

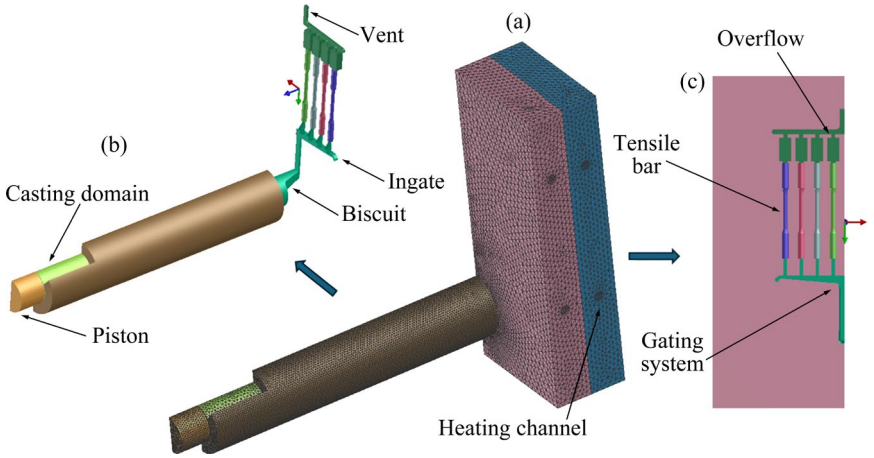

Fig. 3 (a) 1/2 computational domain of entire HPDC machine, (b) detailed view of shot sleeve region and (c) detailed view of die casting region

The three-dimensional Navier−Stokes equations for mass, momentum, and heat transfer are solved using the finite element method. The volume of fluid (VOF) method is employed to model the evolution of the free surface of melt during flow process. The alloy enthalpy curve, calculated using the thermodynamic database provided by ESI, is used to describe the solidification of the alloy melt and the remelting of pre-solidified ESCs.

The porosity formed during solidification is modelled using the POROS model in ProCAST. Moreover, in order to obtain reliable results that are consistent with actual HPDC process, the evolution of die temperatures from room temperature to steady state during the process is modelled based on thermal die cycling approach. A detailed description of this method can be found in our previous work [28].

3.2 Microstructure simulation in shot sleeve

The simulation calculation in shot sleeve is mainly aimed at determining the grain size for ESCs prior to fast injection. The grain size in shot sleeve is calculated based on the fitting equation between grain size and cooling rate obtained with results from the authors. The cooling rate in the shot sleeve before fast injection can be obtained based on the heat transfer and solidification model results in this study, and the evolution diagram of the cooling rate along the length direction of the shot sleeve can be obtained from this.

3.3 Modelling of fluid flow during fast injection and parameters evaluation of shear stress

The Al melt is modeled as an incompressible fluid. The GAS model (ProCAST version 2018.1 User Manual 2018 ESI Group France), which predicts turbulence and fragmentation of the free surface, is employed to qualitatively estimate the amount of entrained air in both the melt and the final casting. Furthermore, the advanced porosity module (APM) is utilized to solve the Darcy equation and address gas segregation in the mushy zone, thereby predicting the distribution of microporosity in the samples.

The calculation formula for shear stress in the flow field is as follows:

$$\tau=\mu\frac{\mathrm{d}u_x}{\mathrm{d}y}+\rho l^2\left(\frac{\mathrm{d}u_x}{\mathrm{d}y}\right)^2 \tag{1}$$

where τ is the shear stress, μ is the viscosity of melt, ρ is the density of melt, l is the Prandtl mixing length, and u_x is the velocity of melt. In this study, the value of u_x is given by flow field calculation.

According to Eq. (1), the expression for calculating shear stress in the model established in this study can be derived, which is given by Eq. (2):

$$\tau=1.3\left(\frac{u_x}{0.0023}\right)+2360\sqrt{0.0008}\sqrt{\frac{u_x}{0.0023}} \tag{2}$$

4 Results and discussion

4.1 Microstructure of pre-solidified products in shot sleeve

The cooling rate is extracted from modelling results of shot sleeve pouring. A sample line is drawn along the longitudinal direction near the inner surface of the shot sleeve. The temperature field and

fraction solid of the shot sleeve, as well as the cooling rate values extracted from the sample line are shown in Fig. 4.

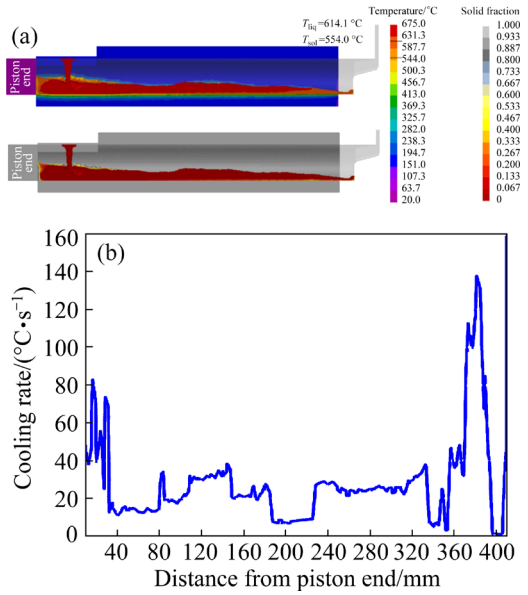

Fig. 4 (a) Temperature field and solid fraction of shot sleeve; (b) Cooling rate along piston

Several studies have suggested that the grain size versus cooling rate variation can be described as an inverse power law relationship [29]. In this work, the relationship between grain size (d) and cooling rate (c) is obtained from an established mathematical model from the authors [30,31] and is shown in Eq. (3). At the numerical simulation results are presented in Fig. 5(b).

$$d=46.94c^{-0.378} \quad (3)$$

In Fig. 5(a), the solidification structures at three positions near the shot sleeve wall are observed using SEM and OM. The three positions are illustrated in Fig. 1. The grain size of these three locations is measured based on the observation results, which are presented by the data points with error bars in Fig. 5(b). The grain size determined by numerical simulation is compared with the experiment values in Fig. 5(b). Because the grain size is proportional to the cooling rate, the faster cooling rate at Position 3 results in a smaller grain size. The simulated grain size at three positions is smaller than the actual measured average, but closer to the lower limit of the measured value. The error between simulation and experiment is less than 20%. Considering the measurement error and the unevenness in the microscopic size, this error is within an acceptable range. The simulation value can be used to reflect the experiment value.

In Fig. 6, the number of grains in shot sleeve under different ESC diameter distributions based on numerical simulation is counted. The number of grains with a diameter ranging from 4.4 to 27.8 μm shows a normal distribution trend, with the highest number of grains in the diameter range of 12.2−16.1 μm, approaching 200. The total number of grains with a diameter greater than 27.8 μm is less than 50. At this point, the size distribution data of

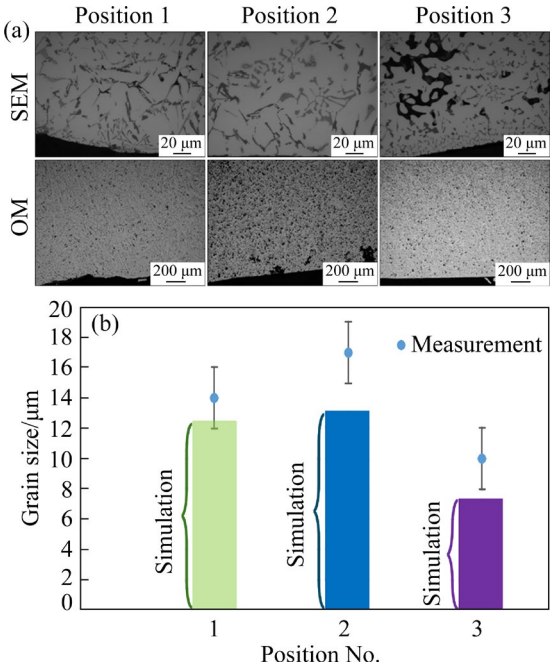

Fig. 5 (a) Solidification structures of shot sleeve wall at Position 1−3; (b) Numerical simulation and measurement results of grain size along shot sleeve

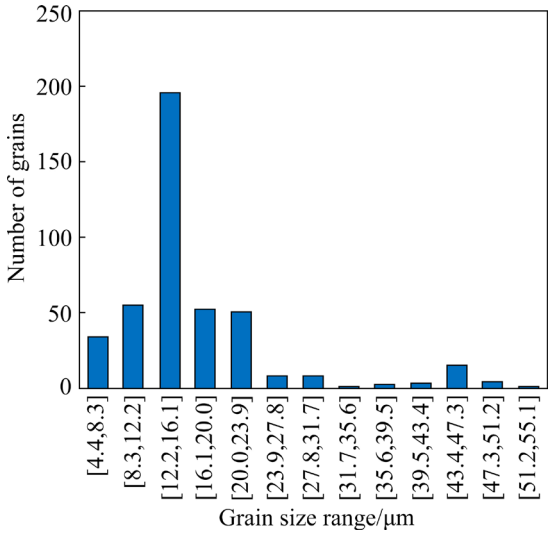

Fig. 6 Number of grains under different ESC diameter distributions (based on numerical simulation)

ESCs are obtained before being subjected to flow shear stress through numerical simulation.

4.2 Numerical simulation of flow shear stress in old and new runners

Table 2 lists the inlet sizes of the new and old runner gating systems, including length, width, and wall thickness. Compared to the old runner, the new runner has a longer flow area and narrower flow channels, which is beneficial for increasing the magnitude of shear stress. In addition, the wall of the new runner is thinner.

Table 2 Inlet sizes of new and old runner gating systems

Runner	Length/m	Width/m	Wall thickness/m
Old	0.040	0.025	0.010
New	0.090	0.020	0.006

Figure 7 shows the numerical simulation of shear stress distribution for new and old runners. In the old runner, the shear stress at the inlet of the gating system is small, about 0.3 MPa. The shear stress in some parts of the tensile sample is relatively high, and the overall stress distribution is very uneven (the maximum is 3 MPa, and the minimum is only 0.3 MPa). Meanwhile, many connections are subjected to high stress due to their compact structure.

The shear stress of the old runner is relatively low and unevenly distributed, which is not conducive to crystal breakage and refinement, and can easily lead to significant differences in the performance of the casting in various parts. In contrast, the shear stress at the inlet of the new runner gating system is high, ranging 2−3 MPa, which is conducive to crystal breakage and refinement. At the same time, the stress distribution at the tensile sample is relatively uniform, and the shear stress in the middle stretching part is 1−2 MPa, which is conducive to the refinement and uniform distribution of casting grains, resulting in excellent casting performance. The new runner has higher overall shear stress, which is more favorable for the fragmentation of ESCs.

4.3 Influence of shear stress on grain size in old and new runners

Figure 8 shows the microstructure of castings (the tensile sample) obtained using new and old runners. The microstructure observations are performed from central samples of the casting system, corresponding to the 3rd and 4th samples for the old runner and the 4th and 5th samples for the new runner. The exact location for observation is the middle section of the tensile sample, as shown in Fig. 7. By comparing the three distinct regions of skin, defect band and centre, the new runner has a finer grain size, while the grain size of the old runner is relatively close to the grain size in Fig. 5(a), indicating that the refinement effect of shear stress is

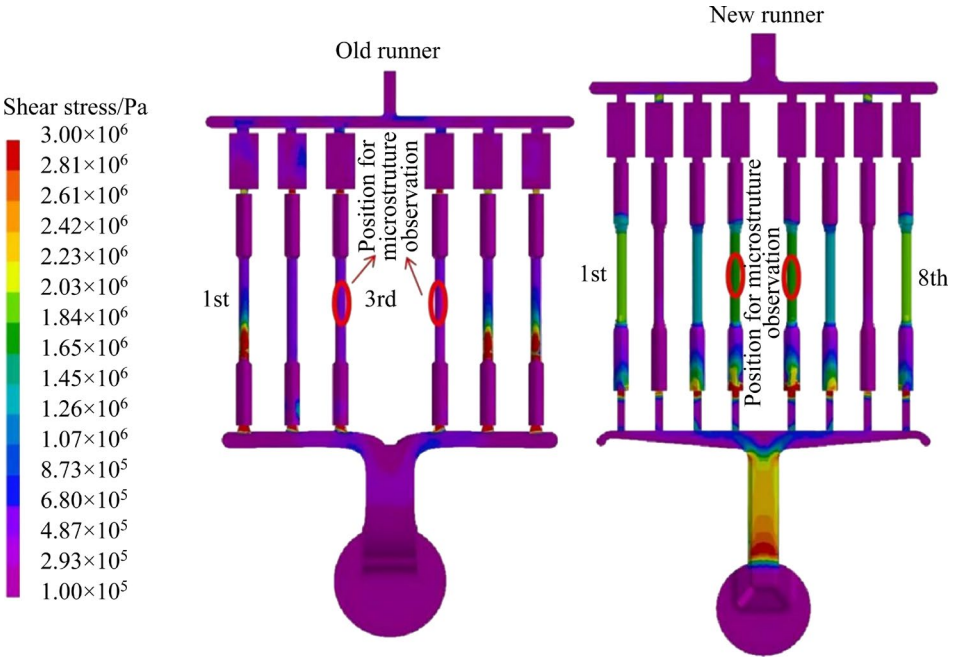

Fig. 7 Numerical simulation results of shear stress on old and new runners

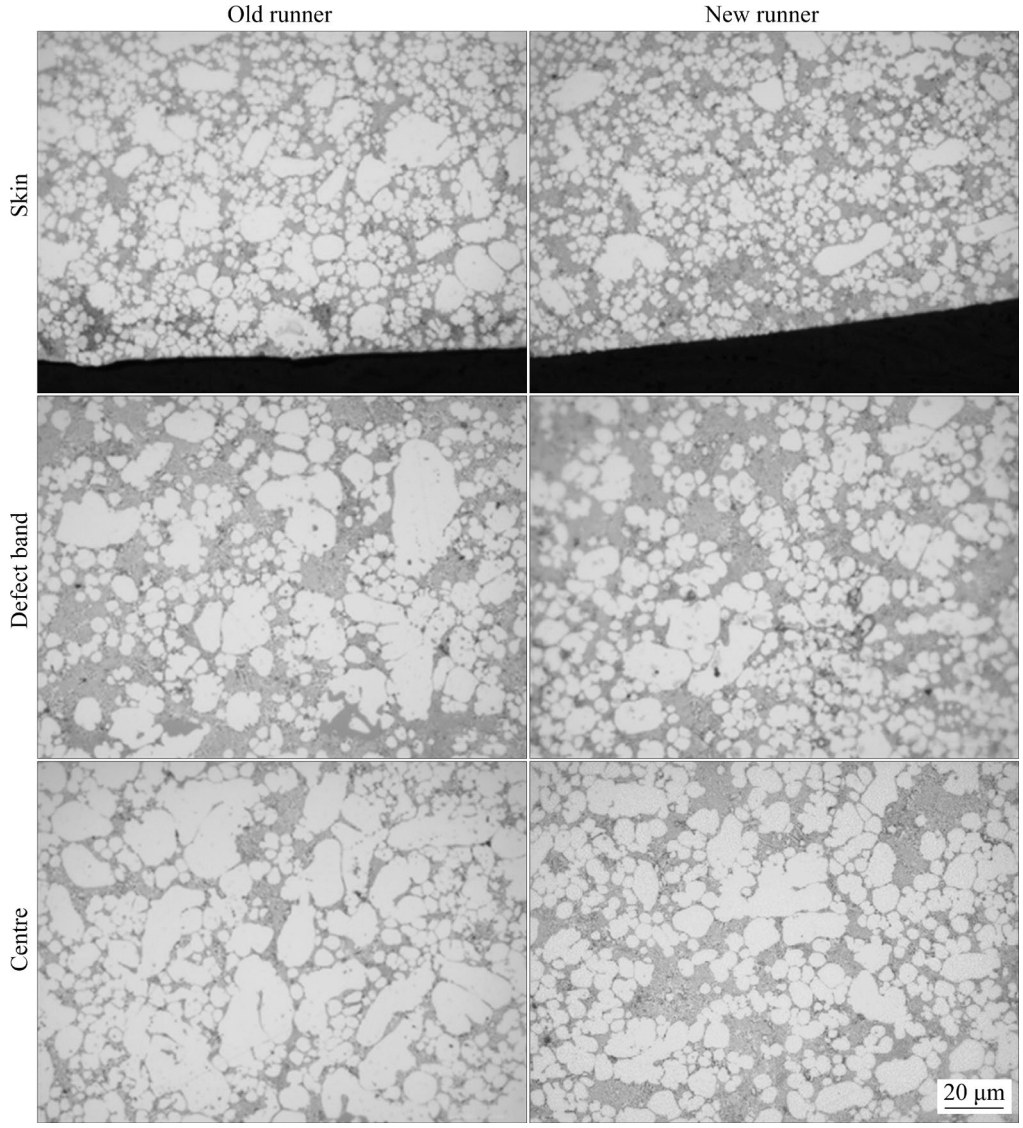

Fig. 8 Microstructure in different regions (skin, defect band, centre) of castings obtained from old and new runners

poor in the old runner. By using a new runner, the overall grain size of the castings obtained by die casting is much smaller than that of the pre-solidified grains inside the shot sleeve, where shear stress plays a crucial role. Overall, replacing the new runner is beneficial for using shear stress to break and refine grains.

4.4 Crystal breakage theoretical model and validation

This model is based on the research on protein breakage during turbulent flow through different flow geometries [32]. And it is further developed based on energy and force balance on a solidified grain under shear flow in a pipe. The energy generated by turbulence eddy dissipation should be large enough to overcome the UTS of the grain to break it. Equations (4)−(8) are the formulas for calculating the grain size after being broken, where Eqs. (4), (5) and (8) are consistent with those in the literature, while Eqs. (6) and (7) are different. The value of k in Eq. (6) is a function of flow velocity, as higher flow velocity leads to more breakage.

$$\Delta D_{50}=k\left(\frac{1}{\varepsilon_{\mathrm{th}}}\right)^{n}(\varepsilon_{\mathrm{i}}-\varepsilon_{\mathrm{th}})\Delta t \tag{4}$$

$$n=0.62\varepsilon_{\mathrm{i}}^{0.1} \tag{5}$$

$$k=0.0001v^{1.10n} \tag{6}$$

$$\varepsilon_{\mathrm{th}}=\frac{A\cdot v\cdot\sigma_{\mathrm{b}}}{M} \tag{7}$$

$$D_{50,\Delta t}=D_{50}^{0}-\Delta D_{50} \tag{8}$$

where $D_{50,\Delta t}$ is the median particle diameter at any

time, μm; D_{50}^{0} is the initial median particle diameter, μm; ΔD_{50} is the total particle breakage; Δt is the residence time increment, s; ε_{th} is the critical turbulence eddy dissipation rate needed to break the grain of a given size, $m^2 \cdot s^{-3}$; ε_i is the cross-section averaged dissipation rate in the runner; A is surface area of particle, m^2; v is particle velocity, m/s; σ_b is tensile strength, MPa; M is mass of particle, kg.

At the same time, orifices of different lengths operate at a given mass flow rate, with the same fluid velocity, but they exhibit different breakage rates, slightly different breakage mechanisms, and different ε_i. Since the breakage mechanism is determined by the level of ε_i, then the k term may be expressed as function of the n term. Therefore, it is suggested that the k term must be a function of both flow velocity and ε_i. The specific equation values are obtained by fitting the experimental results. Equation (7) is obtained based on the tensile strength that needs to be overcome.

Based on this theoretical model, the crystal breakage under shear stress, i.e. the change in grain size, is predicted based on the size of ESCs. Figures 9 and 10 show the theoretical prediction of particle size changes before and after melt shearing in old and new runner, respectively. It can be clearly seen that in the old runner, the particle size hardly changes after melt shearing. In new runner, the particle size decreases significantly after melt shearing, and the larger the original size of the particles is, the more obvious the melt shear effect occurs, and the more the particle size decreases. The smaller particles themselves do not show significant changes, but the effect is still better than the old runner.

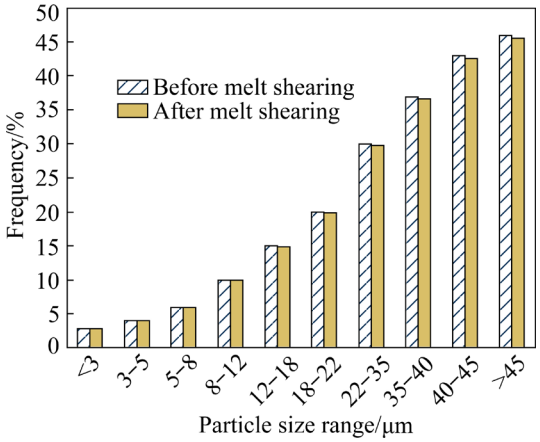

Fig. 9 Theoretical prediction of particle size changes before and after melt shearing in old runner

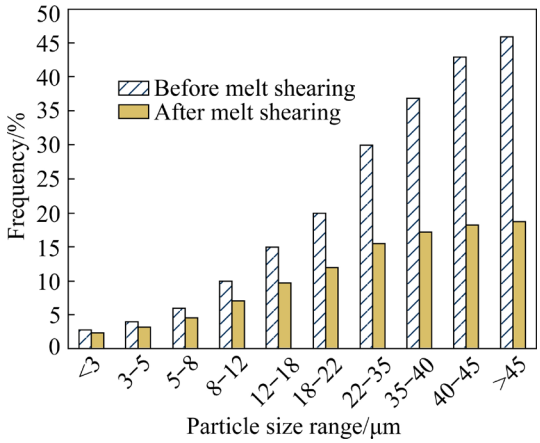

Fig. 10 Theoretical prediction of particle size changes before and after melt shearing in new runner

From the above results, the new runner has a more excellent application for the shear effect of the melt, which is conducive to the uniformity of the microstructure of the casting and the improvement of the casting performance.

Figure 11 shows the grain size values at different locations measured in the old and new runner affected by flow shear stress, as well as the predicted grain size values based on the aforementioned crystal breakage theoretical model. At these three locations, the predicted values correspond well with the measured values, and the prediction results have small errors. Among them, the prediction error of defect band position is the smallest. The predicted results of skin and centre are also within the error range of the measured values. Of course, compared to the other two positions, the prediction error of the center is relatively large, close to 20%. Therefore, future work will consider further reducing the prediction error of the center. In

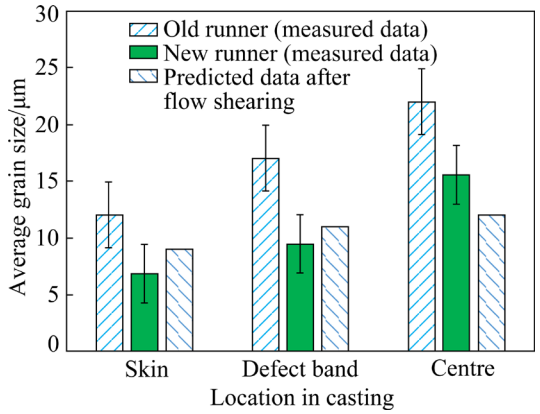

Fig. 11 Measurement and prediction data of average grain size after flow shearing at different positions in casting

summary, it can be considered that the theoretical model has good application in this study.

5 Conclusions

(1) Experiments and numerical simulations were conducted to examine the pre-solidified ESCs in the shot sleeve, with focus on the relationship between grain size and cooling rate. The numerical simulation results for grain size closely align with experimental findings. Grains in the size range of 12.2−16.1 μm constitute a significant proportion of the ESCs and are the primary targets of subsequent shear fragmentation.

(2) Numerical simulations were performed to analyze the shear stress acting on grains in both new and old runner designs, with observations of grain size before and after melt shearing. The simulation results indicate that the new runner generates higher overall shear stress, with a more uniform stress distribution, making it more conducive to ESC fragmentation. Grain observations confirm that replacing the old runner with the new one enhances the use of shear stress for breaking and refining grains.

(3) Drawing inspiration from cell fragmentation processes in medicine, a theoretical model for crystal breakage was established and validated. This model demonstrates excellent predictive accuracy, with its predictions closely match experimental results. It serves as a valuable tool for further in-depth research and plays a significant role in improving the design of die-casting machines and enhancing the quality of die-cast components.

CRediT authorship contribution statement

Jing-zhou LU: Conceptualization, Methodology, Software, Investigation, Formal analysis, Writing − Original draft; **Kun DOU:** Conceptualization, Funding acquisition, Resources, Supervision, Writing − Review & editing; **Yi-jie ZHANG:** Data curation, Visualization; **Ewan LORDAN:** Investigation, Validation; **Alain JACOT:** Investigation, Validation; **Zhongyun FAN:** Resources, Supervision, Software; **Wan-lin WANG:** Resources, Supervision, Software.

Declaration of competing interest

The authors declare that they have no known competing financial interests or personal relationships that could have appeared to influence the work reported in this paper.

Acknowledgments

The financial supports from the National Natural Science Foundation of China (No. 52304360), the Open Foundation of the State Key Laboratory of Advanced Metallurgy, University of Science and Technology Beijing, China (No. K22-07), the Key Research and Development Program of Xiangjiang Laboratory, China (NO. 22XJ01002) and the EPSRC Centre for Innovative Manufacturing in Liquid Metal Engineering, China (The EPSRC Centre-LiME, No. RRR1025R33390) are greatly acknowledged.

References

[1] KOYA E, NAKAGAWA M, KITAGAWA S, ISHIMOTO J, NAKANO Y, OCHIAI N. Research of atomization phenomena in HPDC-step 1 feature of gas porosity dispersion and photography of atomized flow [R]. SAE Technical Papers, 2018: 1−8. https://doi.org/10.4271/2018-01-1392.

[2] SAEEDIPOUR M, SCHNEIDERBAUER S, PIRKER S, BOZORGI S. Numerical simulation of turbulent liquid jet breakup using a sub-grid criterion with industrial application [C]//26th European Conference on Liquid Atomization and Spray Systems. Bremen, Germany, 2014: 1−11.

[3] SAEEDIPOUR M, PIRKER S, SCHNEIDERBAUER S. Numerical study on liquid jet breakup and droplet-wall interaction in high pressure die casting process [C]//Proceedings of ICLASS 2015 (The 13th Triennial International Conference on Liquid Atomization and Spray Systems). Taiwan, China, 2015: 1−11.

[4] YANG Hai-lin, JI Shou-xun, WATSON D, FAN Zhong-yun. Repeatability of tensile properties in high pressure die-castings of an Al−Mg−Si−Mn alloy [J]. Metals and Materials International, 2015, 21: 936−943. https://doi.org/10.1007/s12540-015-5108-0.

[5] DONG Xi-xi, ZHU Xiang-zhen, JI Shou-xun. Effect of super vacuum assisted high pressure die casting on the repeatability of mechanical properties of Al−Si−Mg−Mn die-cast alloys [J]. Journal of Materials Processing Technology, 2019, 266: 105−113. https://doi.org/10.1016/j.jmatprotec. 2018.10.030.

[6] CAO H, WESSÉN M. Characteristics of microstructure and banded defects in die cast AM50 magnesium components [J]. International Journal of Cast Metals Research, 2005, 18: 377−384. https://doi.org/10.1179/136404605225023216.

[7] LAUKLI H I, GOURLAY C M, DAHLE A K, LOHNE O. Effects of Si content on defect band formation in hypoeutectic Al−Si die castings [J]. Materials Science and Engineering A, 2005, 413/414: 92−97. https://doi.org/10.1016/j.msea.2005.08.194.

[8] WU Meng-wu, LI Xiao-bo, GUO Zhi-peng, XIONG Shou-mei. Effects of process parameters on morphology and distribution of externally solidified crystals in microstructure of magnesium alloy die castings [J]. China Foundry, 2018, 15: 139−144. https://doi.org/10.1007/s41230-018-7242-z.

[9] YUAN Zi-hao, GUO Zhi-peng, XIONG Shou-mei. Skin layer of A380 aluminium alloy die castings and its blistering during

solution treatment [J]. Journal of Materials Science & Technology, 2019, 35: 1906−1916. https://doi.org/10.1016/j.jmst.2019.05.011.

[10] NAIK S N, WALLEY S M. The Hall−Petch and inverse Hall−Petch relations and the hardness of nanocrystalline metals [J]. J Mater Sci, 2020, 55: 2661−2681. https://doi.org/10.1007/s10853-019-04160.w.

[11] YANG Yu-tong, HUANG Shi-yao, ZHENG Jiang, YANG Li, CHENG Xiao-nong, CHEN Rui-kai, HAN Wei-jian. Effect of porosity and α-Al(Fe/Mn)Si phase on ductility of high-pressure die-casting Al−7Si−0.2Mg alloy [J]. Transactions of Nonferrous Metals Society of China, 2024, 34: 378−391. https://doi. org/10.1016/S1003-6326(23)66405-2.

[12] HOU Ying-ying, WU Meng-wu, TIAN Bing-hui, LI Xiao-bo, XIONG Shou-mei. Characteristics and formation mechanisms of defect bands in vacuum-assisted high-pressure die casting AE44 alloy [J]. Transactions of Nonferrous Metals Society of China, 2022, 32: 1852−1865. https://doi.org/10.1016/S1003-6326(22)65913-2.

[13] YANG Wen-chao, JI Shou-xun, ZHANG Rui-rong, ZHANG Jun, LIU Lin. Abnormal grain refinement behavior in high-pressure die casting of pure Mg with addition of Zr as grain refiner [J]. JOM, 2018, 70: 2555−2560. https://doi.org/10.1007/s11837-018-3087-6.

[14] LAUKLI H I, ARNBERG L, LOHNE O. Effects of grain refiner additions on the grain structures in HPDC A356 castings [J]. International Journal of Cast Metals Research, 2005, 18: 65−72. https://doi.org/10.1179/136404605225022919.

[15] JI Shou-xun, JIANG Bin, YANG Wen-chao, FAN Zhong-yun. Melt quenched high pressure die casting (MQ-HPDC) of an A356 alloy [J]. Materials Science Forum, 2013, 765: 195−199. https://doi.org/10.4028/www.scientific.net/msf.765.195.

[16] HAGHAYEGHI R, EZZATNESHAN E, BAHAI H, NASTAC L. Numerical and experimental investigation of the grain refinement of liquid metals through cavitation processing [J]. Metals and Materials International, 2013, 19: 959−967. https://doi.org/10.1007/s12540-013-5008-0.

[17] LI Hu-tian, XIA Ming-xu, JARRY P, SCAMANS G M, Fan Zhong-yun. Grain refinement in a AlZnMgCuTi alloy by intensive melt shearing: A multi-step nucleation mechanism [J]. Journal of Crystal Growth, 2011, 314: 285−292. https://doi.org/10.1016/j.jcrysgro.2010.10.168.

[18] FAN Zhong-yun, WANG Yun, XIA Ming-xu, ARUMUGANATHAR S. Enhanced heterogeneous nucleation in AZ91D alloy by intensive melt shearing [J]. Acta Materialia, 2009, 57: 4891−4901. https://doi.org/10.1016/j.actamat.2009.06.052.

[19] KOTADIA H R, BABU N H, ZHANG Hua-wei, FAN Zhong-yun. Microstructural refinement of Al−10.2%Si alloy by intensive shearing [J]. Materials Letters, 2010, 64: 671−673. https://doi.org/10.1016/j.matlet.2009.12.033.

[20] MEN Hua, JIANG B, FAN Zhong-yun. Mechanisms of grain refinement by intensive shearing of AZ91 alloy melt [J]. Acta Materialia, 2010, 58: 6526−6534. https://doi.org/10.1016/j.actamat.2010.08.016.

[21] JIA Zhi-hong, ZHOU Guang-wen, ZHOU Hong-yu, LIU Fei, DING Li-peng, WENG Yao-yao, XIANG Kai-yun, ZHAO Hai-dong. Effects of Cu content and heat treatment process on microstructures and mechanical properties of Al−Si−Mg−Mn−xCu cast aluminum alloys [J]. Transactions of Nonferrous Metals Society of China, 2024, 34: 737−754. https://doi.org/10.1016/S1003-6326(23)66431-3.

[22] GUNASEGARAM D R, FINNIN B R, POLIVKA F B. Melt flow velocity in high pressure die casting: Its effect on microstructure and mechanical properties in an Al−Si alloy [J]. Materials Science and Technology, 2007, 23: 847−856. https://doi.org/10.1179/174328407x176992.

[23] GUNASEGARAM D R, GIVORD M, O'DONNELL R G, FINNIN B R. Improvements engineered in UTS and elongation of aluminum alloy high pressure die through the alteration of runner geometry and plunger velocity [J]. Materials Science and Engineering A, 2013, 559: 276−286. https://doi.org/10.1016/j.msea.2012.08.098.

[24] WANG Bai-shu, XIONG Shou-mei. Effects of shot speed and biscuit thickness on externaly solidified crystals of high-pressure diet cast AM60B magnesium alloy [J]. Transactions of Nonferrous Metals Society of China, 2011, 21: 767−772. https://doi.org/10.1016/S1003-6326(11)60778-4.

[25] LI Xiao-bo, YU Wen-bo, WANG Jun-sheng, XIONG Shou-mei. Influence of melt flow in the gating system on microstructure and mechanical properties of high pressure die casting AZ91D magnesium alloy [J]. Materials Science and Engineering A, 2018, 736: 219−227. https://doi.org/10.1016/j.msea.2018.08.090.

[26] ZHOU Y, GUO Zhi-peng, XIONG Shou-mei. Effect of runner design on the externally solidified crystals in vacuum die-cast Mg−3.0Nd−0.3Zn−0.6Zr alloy [J]. Journal of Materials Processing Technology, 2019, 267: 366−375. https://doi.org/10.1016/j.jmatprotec.2018.12.032.

[27] JIAO X Y, WANG P Y, LIU Yi-xian, LIU Wen-ning, WAN Ao-xiang, SHI L J, WANG C G, XIONG Shou-mei. The characterization of porosity and externally solidified crystals in a high pressure die casting hypoeutectic Al−Si alloy using a newly developed ceramic shot sleeve [J]. Materials Letters, 2024, 360: 136045. https://doi.org/10.1016/j.matlet.2024.136045.

[28] DOU Kun, LORDAN E, ZHANG Yi-jie, JACOT A, FAN Zhong-yun. Understanding the initial solidification behavior for Al−Si alloy in cold chamber high-pressure die casting (CC-HPDC) process combining experimental and modeling approach [J]. Metallurgical and Materials Transactions A, 2022, 53: 3110−3124. https://doi.org/10.1007/s11661-022-06731-0.

[29] SHARIFI P, JAMALI J, SADAYAPPAN K, WOOD J T. Grain size distribution and interfacial heat transfer coefficient during solidification of magnesium alloys using high pressure die casting process [J]. Journal of Materials Science & Technology, 2018, 34: 324−334. https://doi.org/10.1016/j.jmst.2016.09.004.

[30] DOU Kun, LORDAN E, ZHANG Yi-jie, JACOT A, FAN Zhong-yun. A complete computer aided engineering (CAE) modelling and optimization of high pressure die casting (HPDC) process [J]. Journal of Manufacturing Processes, 2020, 60: 435−446. https://doi.org/10.1016/j.jmapro.2020.10.062.

[31] DOU Kun. A novel approach to optimize mechanical properties for aluminium alloy in high pressure die casting (HPDC) process combining experimental and modelling

approach [J]. Journal of Materials Processing Tech, 2021, 296: 117193.
[32] ZUMAETA N, BYRNE E P, FITZPATRICK J J. Breakage of protein precipitates flowing through orifices [J]. Chemical Engineering Research and Design, 2008, 86: 107−117. https://doi.org/10.1016/j.cherd.2007.10.017.

轻合金高压压铸流动剪切致晶粒破碎的数学模型

陆靖洲[1,2]，窦 坤[1,2]，张亦杰[3]，Ewan LORDAN[4]，Alain JACOT[4]，Zhongyun FAN[4]，王万林[1]

1. 中南大学 冶金与环境学院，长沙 410083；
2. 湖南工商大学 湘江实验室，长沙 410205；
3. 栋梁铝业有限公司 新材料研究院，湖州 313008；
4. Brunel Centre for Advanced Solidification Technology (BCAST), Brunel University London, Kingston Lane, Uxbridge, UB8 3PH, United Kingdom

摘 要：在轻合金冷室高压压铸(CC-HPDC)工艺中，快速流动的熔体通过窄流道产生的强剪切应力会破坏外部凝固的晶体(ESC)。在铝合金 CC-HPDC 工艺中应用了两种流道配置来解决该问题。通过有限元模型，计算了模具填充过程中流道区域的剪切应力，并建立了新的晶粒破碎数学模型，用于定量分析不同流道中 ESC 的破碎情况。粒径在 12.2~16.1 μm 之间的颗粒在 ESC 中占很大比例，是随后剪切破碎的主要对象。在 HPDC 测试试验中通过表征铸态样品中的晶粒形貌和尺寸分布来验证数学模型，模型的误差小于 20%。结果表明，该新模型适用于轻合金 CC-HPDC 工艺中的流道系统设计和最佳工艺参数选择。

关键词：外部凝固晶体(ESC)；流动剪切；数学模型；微观结构；高压压铸(HPDC)

(Edited by Bing YANG)